An optimal control approach to imaging by modification

Yves Capdeboscq, Frédéric de Gournay, Jérôme Fehrenbach, Otared Kavian

AN OPTIMAL CONTROL APPROACH TO IMAGING BY MODIFICATION

Y. CAPDEBOSCQ , F. DE GOURNAY , J. FEHRENBACH , AND O. KAVIAN

Abstract. We discuss the reconstruction of the impedance from the local power density. This study is motivated by a new imaging principle which allows to recover interior measurements of the energy density by a non invasive method. We discuss the theoretical feasibility in two dimensions, and propose numerical algorithms to recover the conductivity in two and three dimension. The efficiency of this approach is documented by several numerical simulations.

1. Introduction

Let Ω be a simply connected open set in $\mathbb{R}^d$, $d = 2$ or 3, with a C^1 boundary $\partial\Omega$. Given an integer $N \geq 1$, let $(g_i)_{1\leq i\leq N}$ be N continuous functions in $H^{1/2}(\partial\Omega)$, and given $\sigma \in L^\infty(\Omega)$, consider u_i, solution to the following conductivity problems

$$\operatorname{div}\left(\mathrm{e}^\sigma \nabla u_i\right) = 0 \text{ in } \Omega, \quad u_i = g_i \text{ on } \partial\Omega, \text{ for all } i \in \{1,\dots,N\}, \tag{1}$$

and define $(S_{i,j})_{1\leq i,j\leq N} \in L^1(\Omega)$ by

$$S_{ij} := \mathrm{e}^\sigma \nabla u_i \cdot \nabla u_j \text{ a.e. in } \Omega. \tag{2}$$

This work is devoted to the theoretical and numerical study of the following inverse problem: given the functions $(S_{ij})_{1\leq i,j\leq N}$ on $\omega \subset\subset \Omega$, and given σ near the boundary of the domain, recover σ inside ω.

This question is motivated by a new imaging method for the determination of the conductivity inside the domain Ω, which relies both on electrical impedance tomography and ultrasonic wave focusing. A focused ultrasonic wave modifies slightly the conductivity within the domain, which allows in turn to recover the energy densities S_{ij}. This method is described in the recent work of Ammari *et al.* [2]. In this paper, a first inversion algorithm is proposed to recover e^σ from S_{11}, S_{22} and S_{12}, which recovers data very successfully.

Yet, many questions are left unanswered. In [2], the case of a full energy density map is considered, *i.e.* $\omega = \Omega$, and the *ad-hoc* algorithm proposed cannot be extrapolated simply when imaging smaller subdomains. This algorithm relies in a fundamental way on the existence of several measurements (at least two), and diverges in general for one measurement. Furthermore, because it is based on a perturbation approach, its stability cannot be guaranteed *a priori*.

This problem is studied here from a different perspective, that of optimal control. Consider the case of one current, that is, one data S_{11}. It is clear that the inversion can be reformulated as a minimisation problem, such as the following

$$\text{Minimise } \mathcal{J}(\sigma) := \int_\omega j\left(E(\sigma), x\right) dx \text{ over all } \sigma \in L^\infty(\Omega), \tag{3}$$

where $j : \mathbb{R} \times \Omega \longrightarrow [0,\infty)$ is an appropriately chosen sufficiently smooth function and $j(s,x) = 0$ iff $s = S_{11}(x)$, and

$$E(\sigma) := \mathrm{e}^\sigma |\nabla u|^2 \text{ with } \operatorname{div}\left(\mathrm{e}^\sigma \nabla u\right) = 0 \text{ in } \Omega,\ u = g_1 \text{ on } \partial\Omega. \tag{4}$$

The solving methods and numerical results presented in this paper follow this formulation, or its multi-data counterpart. To assess the quality of the inversion procedure, it is necessary to establish what can be recovered. Note that, even though the problem under consideration is related to electrical impedance tomography, we cannot rely on the theoretical results obtained for that problem: indeed we cannot assume that the Steklov-Poincaré operator, or the Dirichlet-to-Neumann map, is known, since only a limited number of voltage potentials $(g_i)_{1\leq i\leq N}$ are imposed on the boundary.

In fact, the nature of the inversion is quite different. For instance in the one dimensional case in which $\Omega = (0,1)$, with one data S_{11} known everywhere on $(0,1)$, the conductivity is easily determined. Indeed, for some constant C we have $\mathrm{e}^{\sigma}u_x = C$ and thus $S_{11} = \mathrm{e}^{-\sigma}C^2$. Also assuming for instance $g_1(1) - g_1(0) = 1$, one infers that $C\int_0^1 \mathrm{e}^{\sigma(x)}dx = u(1) - u(0) = 1$, and $C = \int_0^1 S_{11}(x)dx$ so that C is determined by S_{11} and finally σ is completely determined. In contrast, using electrical impedance tomography, only the average of the conductivity over $(0,1)$ can be recovered.

Of paramount importance for this complete reconstruction is the knowledge of S_{11} everywhere on $(0,1)$. In any dimension, if the data is only known on a subdomain ω strictly included in Ω, one can only hope to recover the log-conductivity σ up to an additive constant, as it is illustrated by the following example. Suppose for simplicity that $d = 2$ and that the domain is a disk of radius 1 centered at the origin, and that the log-conductivity is radial, given by

$$\sigma \quad = \quad \begin{cases} \log\gamma_0 & \text{if } r < \frac{1}{2} \\ \log\gamma_1 & \text{if } \frac{1}{2} < r < \frac{1}{\sqrt{2}} \\ 0 & \text{if } \frac{1}{\sqrt{2}} < r < 1 \end{cases}.$$

In such a case, for a boundary condition of the form $g = c_1\cos(\theta) + s_1\sin(\theta)$, $\theta \in (0, 2\pi)$, the solution u, and, in turn, the data, can be computed explicitly by separation of variables. The solution u is given in polar coordinates by $u(r,\theta) = p_1\left(c_1\cos(k\theta) + s_1\sin(k\theta)\right)r$, for $r \leq 1/2$, where the constant p_1 is given by

$$p_1 = \frac{16\gamma_1}{\gamma_1^2 + 9\gamma_1 + 3\gamma_1\gamma_0 + 3\gamma_0}.$$

We therefore see that selecting γ_0 and γ_1 of such that $\gamma_0 = \gamma_1(7-\gamma_1)/3(1+\gamma_1)$ will yield the same data as that of an homogeneous medium of log-conductivity $\sigma = 0$. Counter examples for polynomial boundary conditions, $g = \sum_{k=1}^{N} c_k\cos(k\theta) + s_k\sin(k\theta)$ can be constructed similarly by introducing N annulus of different conductivities between the disk of radius $1/2$ and the exterior boundary.

In Section 2, we investigate the theoretical reconstruction of the log-conductivity. First we show that, if $s_1 = \mathrm{e}^{\sigma/2}\nabla u_1$ is known, that is not only the modulus $S_{11}^{1/2}$ but also the direction $\theta_1 := |\nabla u_1|^{-1}\nabla u_1$ of the gradient ∇u_1 is known, then the conductivity may be determined up to a multiplicative constant, under some regularity assumption (this means that the *log-conductivity* σ is determined up to an additive constant). Then, we show that if two *diffeomorphic measurements* s_1 and s_2 are performed, yielding a set of three data S_{11}, S_{22} and S_{12}, the direction θ_1 can also be recovered up to a constant. Note that when $\omega = \Omega$, using the fact that σ is known in a neighbourhood of $\partial\Omega$, both constants involved in the determination of the log-conductivity and that of the direction θ_1 can be recovered. By *diffeomorphic measurements* we mean that the solutions u_1, u_2 satisfy

$$\det(\nabla u_1, \nabla u_2) > 0 \quad \text{or equivalently} \quad \det(s_1, s_2) > 0 \text{ a. e. in } \omega. \tag{5}$$

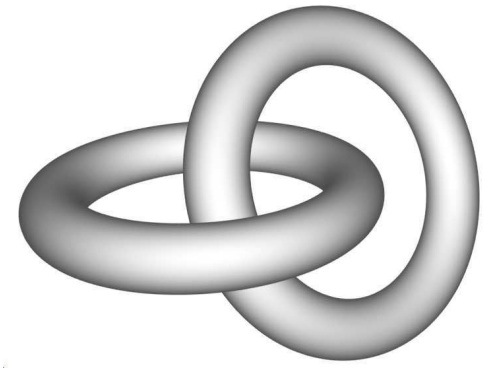

FIGURE 1. A problematic configuration for the conductivity when $d = 3$ and when the conductivity is very high in the annuli compared to that of the background medium.

The difficulty is that we want to ensure that we have performed diffeomorphic measurements by a judicious choice of g_1 and g_2, independently of σ. The following theorem of Alessandrini and Nesi [1], extending the classical theorem of Radò (1926), Kneser (1926), and Choquet (1945) for harmonic maps, shows that in two dimension, there are many such possible choices. We formulate it for the scalar case, although in [1] the result is shown for matrix valued conductivities.

Theorem 1.1 (Alessandrini & Nesi [1])**.** *Let $\Omega \subset \mathbb{R}^2$ be a bounded simply connected open set, whose boundary $\partial\Omega$ is a simple closed curve. Let $\mathbf{g} = (g_1, g_2)$ be a mapping $\partial\Omega \to \mathbb{R}^2$ which is a homeomorphism of $\partial\Omega$ onto a convex closed curve $\mathcal{C}$, and let D denote the bounded convex domain bounded by $\mathcal{C}$. Let $\sigma \in L^\infty(\Omega)$, and let $U = (u_1, u_2)$ be the σ-harmonic mapping whose components u_1, u_2 are solutions of the Dirichlet problems*

$$\begin{aligned} div\,(\mathrm{e}^\sigma \nabla u_i) &= 0 \text{ in } \Omega, \\ u_i &= g_i \text{ on } \partial\Omega, \end{aligned}$$

with $g_i \in H^1(\Omega) \cap C(\overline{\Omega})$ and $i = 1, 2$. Then U is a homeomorphism of $\overline{\Omega}$ onto $\overline{D}$. In particular we have either

$$\forall\, \omega \subset\subset \Omega,\ \det(\nabla u_1, \nabla u_2) > 0 \quad a.e.\ in\ \omega$$

or

$$\forall\, \omega \subset\subset \Omega,\ \det(\nabla u_1, \nabla u_2) < 0 \quad a.e.\ in\ \omega$$

As a consequence, assuming that Ω is convex and sufficiently smooth, taking measurements with, say, $g_1 = x_1$ and $g_2 = x_2$ (that is $\mathbf{g} = Id$), we are guaranteed that condition (5) holds.

Unfortunately, such a result is not true when $d = 3$, even in the harmonic case as it was proved by Laugesen [5], and changes of signs in the determinant can happen arbitrarily small scales, see Briane *et al.* [3]. Geometries such as the one sketched in Figure 1 provide counter-examples. These results indicate that an extension of our approach of the uniqueness problem to the three dimensional case is likely to fail.

In Section 3, we adopt an optimisation point of view, and consider the inverse problem as described in (3). More precisely, we introduce two functionals

$$\mathcal{J}_1(\sigma) := \int_\omega \left(\mathrm{e}^{\sigma/2}\,|\nabla u| - S_{11}^{1/2}\right)^2,$$

and

$$\mathcal{J}_2(\sigma) := \frac{1}{2}\sum_{i=0}^{n}\left(\int_{\omega_i} \mathrm{e}^{\sigma}\,|\nabla u|^2\,dx - \int_{\omega_i} S_{11}\,dx\right)^2,$$

where $(\omega_i)_{1\le i\le n}$ is a partition of ω. We compute their differentials, and show that strict convexity of such functionals cannot be guaranteed *a priori.* This fact is not related to the particular choice of integrand (cost functions j in the language of optimal control (3)). We then discuss how a weaker lower bound on the Hessian can be used to improve minimisation procedures, and why several electric measurements are beneficial.

For the sake of concision, the gradient descent method used to minimise $\mathcal{J}_1$ is not detailed. In Section 4, we detail the implementation of the Gauss-Newton method used to minimise $\mathcal{J}_2$. For an increased numerical efficiency, the Jacobian matrix of the cost function is evaluated differently on fine and coarse meshes. This leads to a multigrid algorithm. For three dimensional computations, the involved number of degrees of freedom prohibits the resolution of very fine scale problems. We believe that our algorithm, because it is multigrid, allows to circumvent this difficulty, if a fine resolution is needed only in a small area of the domain.

Finally in Sections 5 and 6, numerical examples are presented and discussed. In the two dimensional case, with the idea of a patchwork resolution in mind, we document how parallel resolution on different patches can be performed. In the three dimensional case the multi-grid resolution method is illustrated on a half sphere — a domain resembling a breast, since breast cancer detection is an application we have in mind.

2. On the theoretical reconstruction of the conductivity in two dimensions.

In this section we show that, possibly up to two constant parameters, the conductivity can be determined from two diffeomorphic measurements. In fact, we could exhibit an explicit inversion formula from Proposition 2.1 and Proposition 2.2, using formulae (9) and (18), which would simplify the inversion to the evaluation of two real parameters, easily found from the near boundary information available for σ. We chose not to do so for two reasons. First these formulae are exclusively two dimensional, as they rely in an essential way on the fact that divergence free fields are curls, and Theorem 1.1 is used frequently. Finally, both (9) and (18) require to differentiate the measured data, and this is a well known source for instability.

Proposition 2.1. *Assume $d = 2$ and $\sigma \in L^\infty(\Omega)$ be such that $\nabla\sigma \in L^p(\Omega)$ for some $p > 2$. Let u_1 be the solution of (1) for $i = 1$. Assume that $S_{11} \neq 0$ and furthermore that $s_1 := \mathrm{e}^{\sigma/2}\nabla u_1$ is known almost everywhere in $\omega \subset \Omega$, and that*

$$|\nabla u_1|^{-1} \in L^2(\Omega) \quad \text{and} \quad |\nabla u_1|^{-2}\partial_{ij}u_1 \in L^2(\Omega) \tag{6}$$

Then σ is known in ω up to an additive constant. Without further assumptions, the additive constant cannot always be determined.

Proof. Let $\varphi \in H^1_0(\Omega)$ be a test function. Testing (1) against φ we obtain

$$\int_\Omega \mathrm{e}^{\sigma/2} s_1 \cdot \nabla\varphi\,dx = 0.$$

Define

$$J := \begin{bmatrix} 0 & -1 \\ 1 & 0 \end{bmatrix}.$$

Then, using the fact that the vector valued function $\mathrm{e}^{-\sigma/2}s_1$ is a gradient, and that we are in two dimensions, we obtain

$$\int_\Omega \mathrm{e}^{-\sigma/2} Js_1 \cdot \nabla\varphi \, dx = 0.$$

This yields for all test functions φ,

$$\int_\Omega s_1 \cdot \nabla\varphi \, dx - \frac{1}{2}\int_\Omega \nabla\sigma \cdot s_1\varphi \, dx = 0, \tag{7}$$

and

$$\int_\Omega Js_1 \cdot \nabla\varphi \, dx + \frac{1}{2}\int_\Omega \nabla\sigma \cdot Js_1\varphi \, dx = 0. \tag{8}$$

(At this point note that since we assume $\nabla\sigma \in L^p(\Omega)$ and since by Sobolev imbeddings theorem we have $\varphi \in L^q(\Omega)$ for all $q < \infty$ and all $\varphi \in H^1_0(\Omega)$, upon choosing appropriately q one checks that $\nabla\sigma \cdot s_1\varphi \in L^1(\Omega)$). Using the fact that

$$\nabla\sigma = (\nabla\sigma \cdot s_1)\,\frac{s_1}{S_{11}} + (\nabla\sigma \cdot Js_1)\,\frac{Js_1}{S_{11}} \text{ a.e. in } \Omega,$$

for any $\Phi := (\varphi_1, \varphi_2) \in (C^1_c(\Omega))^2$ we obtain

$$\begin{aligned}
\frac{1}{2}\int_\Omega \sigma \mathrm{div}\,(\Phi)\, dx &= -\frac{1}{2}\int_\Omega \nabla\sigma \cdot \Phi \, dx \\
&= -\frac{1}{2}\int_\Omega (\nabla\sigma \cdot s_1)\,\frac{s_1}{S_{11}} \cdot \Phi \, dx - \frac{1}{2}\int_\Omega (\nabla\sigma \cdot Js_1)\,\frac{Js_1}{S_{11}} \cdot \Phi \, dx \\
&= -\int_\Omega s_1 \cdot \nabla\left(\frac{s_1}{S_{11}} \cdot \Phi\right) dx + \int_\Omega Js_1 \cdot \nabla\left(\frac{Js_1}{S_{11}} \cdot \Phi\right) dx\,, \qquad (9)
\end{aligned}$$

where we have used (7) with $\varphi := \Phi \cdot s_1/S_{11}$ and (8) with $\varphi := \Phi \cdot Js_1/S_{11}$. Indeed this is possible, since using the assumption that $\nabla\sigma \in L^p(\Omega)$ while $|\nabla u_1|^{-1} \in L^2(\Omega)$ and $|\nabla u_1|^{-2}\partial_{ij}u_1 \in L^2(\Omega)$ one may check that the defined functions φ are in $H^1_0(\Omega)$.

Now note that the right hand side of (9) depends only on the data s_1: therefore by choosing the support of Φ in ω, that is where s_1 is known, we conclude that the left hand side is known. This in turn proves that σ is known in ω up to an additive constant. □

The proof of proposition 2.1 uses the fact that two orthogonal projections of the flux s_1 can be related to the conductivity. In the next proposition we show that two distinct measurements, yielding three data S_{11}, S_{22} and S_{12} allow to recover the direction $\theta_1 := |\nabla u_1|^{-1}\nabla u_1$ up to a constant, (and in turn, the conductivity using proposition 2.1). This relies on the fact that, provided Ω is convex and smooth, if $g_1 = x_1$ and $g_2 = x_2$, then the solutions u_1, u_2 of (1) verify

$$\det(\nabla u_1, \nabla u_2) > 0 \text{ a.e. in } \omega, \tag{10}$$

thanks to Theorem 1.1.

Proposition 2.2. *Assume that Ω is convex and smooth, that $g_1 = x_1$ and $g_2 = x_2$ so that (10) holds. Assume that S_{11}, S_{22} and S_{12} are known in $\omega \subset \Omega$, and that u_1, u_2 satisfy (6). Then the direction*

$$\theta_1 := \frac{\nabla u_1}{|\nabla u_1|} = \frac{s_1}{|s_1|} = S_{11}^{-1/2}\mathrm{e}^{\sigma/2}\nabla u_1$$

is known up to a constant rotation.

Proof. First, note that $s_1 = \mathrm{e}^{\sigma/2}\nabla u_1$ and $s_2 = \mathrm{e}^{\sigma/2}\nabla u_2$ are related via two known constants. Indeed we may write, for some $\alpha(x), \beta(x)$ that $s_2(x) = \alpha(x)s_1 + \beta(x)Js_1$ and since $\det(s_1, s_2) = s_1 \wedge s_2$ we have

$$s_2 = \alpha(x)s_1 + \beta(x)Js_1 = \frac{S_{12}}{S_{11}}s_1 + \frac{\det(s_1, s_2)}{S_{11}}Js_1. \tag{11}$$

The determinant $\det(s_1, s_2)$ is known, since thanks to (10) its sign is known to be positive (for instance), and therefore

$$\det(s_1, s_2) = \sqrt{S_{11}S_{22} - (S_{12})^2}.$$

From equation (1), and the fact that $d = 2$, we deduce that for any compactly supported test function φ, since for $j = 1, 2$ we have $\mathrm{div}(\mathrm{e}^{\sigma/2}s_j) = 0$, thanks to (11),

$$\int_\Omega \mathrm{e}^{\sigma/2} s_1 \cdot \nabla\varphi \, dx = 0, \tag{12}$$

$$\int_\Omega \mathrm{e}^{\sigma/2} \left(\alpha s_1 + \beta Js_1\right) \cdot \nabla\varphi \, dx = 0, \tag{13}$$

and due to the fact that $\mathrm{e}^{-\sigma/2}s_j$ is a gradient and $Js_2 = \alpha Js_1 - \beta s_1$,

$$\int_\Omega \mathrm{e}^{-\sigma/2} Js_1 \cdot \nabla\varphi \, dx = 0, \tag{14}$$

$$\int_\Omega \mathrm{e}^{-\sigma/2} \left(\alpha Js_1 - \beta s_1\right) \cdot \nabla\varphi \, dx = 0. \tag{15}$$

Assume momentarily that σ, s_1 and s_2 are smooth enough so that we can integrate by parts (13) and (15). Then using the fact that $\mathrm{div}(\mathrm{e}^{-\sigma/2}Js_1) = 0$, we obtain

$$\int_\Omega \mathrm{e}^{\sigma/2}\nabla\alpha \cdot s_1\varphi \, dx + \int_\Omega \mathrm{e}^{-\sigma/2}\nabla\left(\mathrm{e}^{\sigma}\beta\right) \cdot Js_1\varphi \, dx = 0,$$

and

$$\int_\Omega \mathrm{e}^{-\sigma/2}\nabla\alpha \cdot Js_1\varphi \, dx - \int_\Omega \mathrm{e}^{\sigma/2}\nabla\left(\mathrm{e}^{-\sigma}\beta\right) \cdot s_1\varphi \, dx = 0.$$

Introducing $\mathcal{U} = (\nabla\alpha - J\nabla\beta)\beta^{-1}$, we have proved that

$$\int_\Omega \mathcal{U} \cdot s_1\varphi \, dx + \int_\Omega \nabla\sigma \cdot Js_1\varphi \, dx = 0 = \int_\Omega \mathcal{U} \cdot Js_1\varphi \, dx - \int_\Omega \nabla\sigma \cdot s_1\varphi \, dx. \tag{16}$$

Integrating by parts (12), we deduce from (16) the identity,

$$-2\int_\Omega \mathrm{div}\left(s_1\right)\varphi \, dx = \int_\Omega \nabla\sigma \cdot s_1\varphi \, dx = \int_\Omega \mathcal{U} \cdot Js_1\varphi \, dx,$$

and similarly, starting from (14), thanks to (16) we obtain,

$$-2\int_\Omega \mathrm{div}\left(Js_1\right)\varphi \, dx = -\int_\Omega \nabla\sigma \cdot Js_1\varphi \, dx = \int_\Omega \mathcal{U} \cdot s_1\varphi \, dx.$$

Finally we have proved that for any $\Phi = (\varphi_1, \varphi_2) \in C_0^\infty(\Omega)^2$,

$$\begin{aligned}
\int_\Omega \mathcal{U} \cdot J\Phi &= \int_\Omega \left(\mathcal{U} \cdot s_1\right)\left(\frac{J\Phi \cdot s_1}{S_{11}}\right) + \left(\mathcal{U} \cdot Js_1\right)\left(\frac{J\Phi \cdot Js_1}{S_{11}}\right) dx, \\
&= -2\int_\Omega \left(\mathrm{div}\left(Js_1\right)\frac{J\Phi \cdot s_1}{S_{11}} + \mathrm{div}\left(s_1\right)\frac{J\Phi \cdot Js_1}{S_{11}}\right) dx, \\
&= 2\int_\Omega \left(\mathrm{div}\left(Js_1\right)\frac{Js_1}{S_{11}} + \mathrm{div}\left(s_1\right)\frac{s_1}{S_{11}}\right) \cdot \Phi \, dx.
\end{aligned}$$

A direct computation shows that if we set $\theta_1 := s_1/|s_1|$, and $\theta_1 = (\cos t, \sin t)$, we have

$$\int_\Omega \left(\operatorname{div}(Js_1) \frac{Js_1}{S_{11}} + \operatorname{div}(s_1) \frac{s_1}{S_{11}} \right) \cdot \Phi \, dx = \int_\Omega (-J\nabla t + \nabla(\log S_{11})) \cdot \Phi \, dx, \tag{17}$$

or equivalently

$$\int_\Omega J\nabla t \cdot \Phi \, dx = -\int_\Omega \left(\operatorname{div}(Js_1) \frac{Js_1}{S_{11}} + \operatorname{div}(s_1) \frac{s_1}{S_{11}} - \nabla(\log S_{11}) \right) \cdot \Phi \, dx. \tag{18}$$

Thus we have expressed ∇t in terms of known quantities. To conclude the proof, notice that with the regularity conditions assumed about u_1, u_2, σ, the integrals involving $\mathcal{U}$ and $\nabla(\log S_{11})$ are well defined, and therefore t is determined up to an additive constant. □

3. An optimal control approach

In Section 2, we presented Propositions 2.1 and 2.2 to document the feasibility of the inversion in an ideal case. For the practical inversion, which will be discussed in the sequel, we will adopt a very different approach. The inversion is considered as a minimisation problem, and it is performed in two or three dimensions. In Subsection 3.1, the minimisation problems are precisely stated. The direct and adjoint differentiation of the cost functions are detailed in Subsection 3.2. Numerical simulations are presented in Sections 5 and 6, where several boundary conditions are simultaneously considered and the effective cost functions are sum of cost functions similar to $\mathcal{J}_1$ or $\mathcal{J}_2$. Subsection 3.3 is devoted to the study of the convexity properties of the cost functions. We consider the general form (3) of the minimisation problem, and discuss the convexity properties of the minimisation of

$$\mathcal{J}(\sigma) = \int_\Omega j(E(\sigma), x) \, dx. \tag{19}$$

As in (3), we assume that $j : \mathbb{R} \times \Omega \to L^1(\Omega)$ is a Caratheodory function which is C^2 with respect to its first variable, non-negative, and such that $j(s, x) = 0$ if and only if $s = \mathrm{e}^{\sigma^\star(x)} |\nabla u_\star(x)|^2$, where $\mathrm{e}^{\sigma^\star}$ is the true conductivity and $u_\star$ is the associated electric potential. Strictly convex functionals are known to be favourable in optimisation problems, as they imply uniqueness of the solution and convergence of descent algorithms. We show that the minimisation is not fault free, namely, around the global minimiser, the Hessian of $\mathcal{J}$ is not positive definite.

3.1. **The minimisation problems.** We assume that the true log-conductivity $\sigma^\star$ is known in a layer of positive thickness close to the boundary $\partial\Omega$. More precisely: we assume that $\sigma^\star$ is known in $\Omega \setminus \Omega'$, where Ω' is a subdomain such that $\operatorname{dist}(\Omega', \partial\Omega) > 0$. Let $g \in H^{1/2}(\partial\Omega)$. The set of admissible log-conductivities is

$$L^\infty_{\mathrm{ad}}(\Omega) = \{\sigma \in L^\infty(\Omega) \mid \sigma|_{\Omega\setminus\Omega'} = \sigma^\star\},$$

and its tangent space at any point is the subspace denoted by

$$L^\infty_0(\Omega) = \{\delta \in L^\infty(\Omega) \mid \delta|_{\Omega\setminus\Omega'} = 0\}.$$

If $\sigma \in L^\infty_{\mathrm{ad}}(\Omega)$, we denote by $u(\sigma) \in H^1$ the solution u of

$$\begin{cases} \nabla \cdot (\mathrm{e}^\sigma \nabla u) = 0 & \Omega \\ u = g & \partial\Omega. \end{cases} \tag{20}$$

We describe two optimisation methods to recover the conductivity from energy density measurements. The heuristic idea is to find $\sigma \in L^\infty_{\mathrm{ad}}(\Omega)$ such that

$$E(\sigma) := \mathrm{e}^\sigma |\nabla u|^2$$

approaches $S = E(\sigma^\star)$. For the sake of concision we write sometimes $E(\sigma)$ instead of $E(\sigma, x) = \mathrm{e}^{\sigma(x)}|\nabla u(x)|^2$.

The first method uses local measurements of S on the subdomain ω: it consists in minimising the following cost function

$$\mathcal{J}_1(\sigma) = \int_\omega \left[\sqrt{E(\sigma)} - \sqrt{E(\sigma^\star)}\right]^2 dx. \tag{21}$$

This corresponds to the general problem (19) with $j(s,x) = \left(\sqrt{s} - \sqrt{E(\sigma^\star, x)}\right)^2$ for $x \in \omega$ and $j(s,x) = 0$ otherwise.

The second method is a multigrid method. The domain Ω' is partitioned in subdomains $(\omega_i)_{1\le i\le n}$. Let $\omega_0 = \Omega \setminus \Omega'$. We assume that the total power in each ω_i $(i = 0 \dots n)$ is known, this quantity is $\displaystyle\int_{\omega_i} E(\sigma^\star)$. The cost function to be minimised is:

$$\mathcal{J}_2(\sigma) = \frac{1}{2}\sum_{i=0}^{n}\left(\int_{\omega_i} E(\sigma)\,dx - \int_{\omega_i} E(\sigma^\star)\,dx\right)^2, \tag{22}$$

where we restrict to conductivities that are constant on each ω_i. Note that if a finite element method with piecewise constant conductivities on a mesh $(T_i)_{1\le i\le M}$ is used for the discretisation of (19) with $j(s,x) = (s - E(\sigma^\star, x))^2$, then the minimisation problem of (19) and the minimisation of $\mathcal{J}_2$ are equivalent when $n = M$ and for all $i \in \{1, \dots, M\}$, $\omega_i = T_i$.

To minimise these functionals, we shall use either a steepest descent algorithm with $\mathcal{J}_1$, or a Gauss-Newton algorithm with $\mathcal{J}_2$. Both approaches require differentiations.

3.2. **Differentiation of $\mathcal{J}_1$ and $\mathcal{J}_2$.** It is well known that the mapping $\sigma \mapsto u(\sigma)$ defined on $L^\infty_{\mathrm{ad}}(\Omega) \to H^1(\Omega)$ is C^∞ (in fact analytic), and that if $\delta \in L^\infty_0(\Omega)$, the differential of u in the δ direction is $\mathrm{d}u.\delta = v$ where $v \in H^1_0(\Omega)$ is the solution of the variational problem

$$v \in H^1_0(\Omega), \quad \forall\, \varphi \in H^1_0(\Omega), \qquad \int_\Omega \mathrm{e}^\sigma \nabla v \nabla \varphi\, dx = -\int_\Omega \delta \mathrm{e}^\sigma \nabla u \nabla \varphi\, dx. \tag{23}$$

Consider the mapping

$$\begin{array}{rccc} E: & L^\infty_{\mathrm{ad}}(\Omega) & \longrightarrow & L^1(\Omega) \\ & \sigma & \longmapsto & \mathrm{e}^\sigma |\nabla u(\sigma)|^2. \end{array}$$

The mapping E is clearly differentiable, and its derivative in the δ direction is given by:

$$\mathrm{d}E.\delta = \delta \mathrm{e}^\sigma |\nabla u|^2 + 2\mathrm{e}^\sigma \nabla u \nabla v, \tag{24}$$

where $v = \mathrm{d}u.\delta$ is the unique solution of (23).

Proposition 3.1. *The operator $\mathrm{d}E : L^\infty_0(\Omega) \to L^1(\Omega)$ has the following symmetry property: for all $\delta, \eta \in L^\infty_0(\Omega)$, denoting by $\langle\cdot,\cdot\rangle$ the duality between $L^1(\Omega)$ and $L^\infty(\Omega)$ we have*

$$\langle \mathrm{d}E.\delta, \eta\rangle = \langle \mathrm{d}E.\eta, \delta\rangle.$$

Proof. If $\eta \in L^\infty_0(\Omega)$, then

$$\mathrm{d}E.\eta = \eta \mathrm{e}^\sigma |\nabla u(\sigma)|^2 + 2\mathrm{e}^\sigma \nabla u(\sigma).\nabla w,$$

where w solves

$$\left\{\begin{array}{ll} \nabla\cdot(\mathrm{e}^\sigma \nabla w) = -\nabla\cdot(\eta \mathrm{e}^\sigma \nabla u(\sigma)) & \Omega \\ w = 0 & \partial\Omega. \end{array}\right. \tag{25}$$

We can write

$$\langle \mathrm{d}E.\delta, \eta\rangle_{L^1,L^\infty(\Omega)} = \int_\Omega \eta\delta \mathrm{e}^\sigma |\nabla u(\sigma)|^2 + 2\eta \mathrm{e}^\sigma \nabla u(\sigma).\nabla v.$$

The second term in this integral is evaluated by:

$$\int_\Omega \eta \mathrm{e}^\sigma \nabla u(\sigma).\nabla v = -\int_\Omega v\nabla\cdot(\eta \mathrm{e}^\sigma \nabla u(\sigma)) = -\int_\Omega \mathrm{e}^\sigma \nabla v.\nabla w.$$

As a result,

$$\langle \mathrm{d}E.\delta, \eta\rangle_{L^1,L^\infty(\Omega)} = \int_\Omega \eta\delta \mathrm{e}^\sigma |\nabla u(\sigma)|^2 - 2\int_\Omega \mathrm{e}^\sigma \nabla v.\nabla w.$$

This quantity being symmetric in δ and η, it follows that

$$\langle \mathrm{d}E.\delta, \eta\rangle_{L^1,L^\infty(\Omega)} = \langle \mathrm{d}E.\eta, \delta\rangle_{L^1,L^\infty_0(\Omega)}$$

and the result is proved. □

As a consequence of (23), if we write

$$\mathcal{J}_2(\sigma) = \frac{1}{2}||F(\sigma)||^2,$$

where

$$F(\sigma) = (f_i(\sigma))_{0\le i\le n} \in \mathbb{R}^{n+1} \quad \text{with} \quad f_i(\sigma) = \int_{\omega_i} E(\sigma) - \int_{\omega_i} E(\sigma^\star), \tag{26}$$

the mapping $F : L^\infty_{\mathrm{ad}}(\Omega) \to \mathbb{R}^{n+1}$ defined in (26) is differentiable, and if $\sigma \in L^\infty_{\mathrm{ad}}(\Omega)$ and $\delta \in L^\infty_0(\Omega)$:

$$\mathrm{d}F.\delta = (\mathrm{d}f_0.\delta, \mathrm{d}f_1.\delta, \dots, \mathrm{d}f_n.\delta),$$

with

$$\mathrm{d}f_i.\delta = \int_{\omega_i} \left(\delta + 2\frac{\nabla u(\sigma).\nabla v}{|\nabla u(\sigma)|^2}\right) \mathrm{e}^\sigma |\nabla u(\sigma)|^2\, dx, \tag{27}$$

where v solves (23).

Let us now study the adjoint differentiation of $\mathcal{J}_1$, and $\mathcal{J}_2$.

Proposition 3.2. *Assume that $\omega \subset \Omega'$. Let χ be the characteristic function of ω. Define an error function*

$$\varepsilon(\sigma) := \chi \mathrm{e}^\sigma \left(\sqrt{\frac{E(\sigma^\star)}{E(\sigma)}} - 1\right),$$

and let p be the adjoint state solution of the variational problem

$$p \in H^1_0(\Omega), \quad \forall \varphi \in H^1_0(\Omega) \qquad \int_\Omega \mathrm{e}^\sigma \nabla p \nabla \varphi\, dx = \int_\Omega \varepsilon \nabla u \nabla \varphi\, dx.$$

The functional $\mathcal{J}_1$ is differentiable with respect to σ and its derivative is given by

$$\mathrm{d}\mathcal{J}_1.\delta = \int_\Omega \delta \left(-\varepsilon + 2\frac{\nabla u \nabla p}{|\nabla u|^2}\right) \mathrm{e}^\sigma |\nabla u|^2\, dx. \tag{28}$$

Proof. Note that $p \in H^1_0(\Omega)$ is solution to the elliptic adjoint problem $\mathrm{div}(\mathrm{e}^\sigma \nabla p) = \mathrm{div}(\varepsilon(\sigma)\nabla u)$. We have

$$\mathcal{J}_1(\sigma) = \int_\Omega \chi \left(\sqrt{E(\sigma)} - \sqrt{E(\sigma^\star)}\right)^2 dx$$

and so the derivative of $\mathcal{J}_1$ is:

$$\mathrm{d}\mathcal{J}_1.\delta = \int_\Omega \chi \left(\sqrt{E(\sigma)} - \sqrt{E(\sigma^\star)}\right) \left(\delta \mathrm{e}^{\sigma/2}|\nabla u| + 2\mathrm{e}^{\sigma/2}\frac{\nabla v \nabla u}{|\nabla u|}\right) dx, \tag{29}$$

where $v = \mathrm{d}u.\delta$ is defined in equation (23). In order to write the derivative $\mathrm{d}\mathcal{J}_1$ in terms of δ only — and not in terms of δ and v — an adjoint problem is used. Namely let $p \in H_0^1$ be the solution of:

$$p \in H_0^1(\Omega), \quad \forall\, \varphi \in H_0^1(\Omega)$$
$$\int_\Omega \mathrm{e}^\sigma \nabla p \nabla \varphi \, dx = -\int_\Omega \chi \left(\sqrt{E(\sigma)} - \sqrt{E(\sigma^\star)}\right) \mathrm{e}^{\sigma/2} \frac{\nabla u \nabla \varphi}{|\nabla u|} \, dx = \int_\Omega \varepsilon \nabla u \cdot \nabla \varphi \, dx, \tag{30}$$

Then, choosing $\varphi := v$ in equation (30), it follows from equation (23) with $\varphi = p$ that:

$$\mathrm{d}\mathcal{J}_1.\delta = \int_\Omega \left(\chi \mathrm{e}^\sigma |\nabla u|^2 \left(1 - \sqrt{E(\sigma^\star)/E(\sigma)}\right) + 2\mathrm{e}^\sigma \nabla u \nabla p\right) \delta \, dx,$$

which is (28). □

Proposition 3.3. *Let $\sigma \in L^\infty_{\mathrm{ad}}(\Omega)$ and $Z = (z_0, z_1, \ldots, z_n) \in \mathbb{R}^{n+1}$. Then*

$$\mathrm{d}F^T.Z = z|\nabla u|^2 + 2\nabla u \nabla p \ , \tag{31}$$

where z is the piecewise constant function equal to z_i in ω_i $(i = 0 \ldots, n)$ and p solves

$$\begin{cases} \nabla \cdot (\mathrm{e}^\sigma \nabla p) = \nabla \cdot (z \mathrm{e}^\sigma \nabla u) & \Omega \\ p = 0 & \partial\Omega. \end{cases} \tag{32}$$

This for instance allows us to compute the gradient of the cost-function $\mathcal{J}_2$. Indeed, since $\mathcal{J}_2(\sigma) = \dfrac{1}{2}||F||^2$ we have

$$\nabla \mathcal{J}_2 = \mathrm{d}F^T.F$$

and so it suffices to apply (31) with $Z = F$.

Proof of Proposition 3.3. If $\delta \in L^\infty_0(\Omega)$, then

$$\langle \mathrm{d}F^T.Z, \delta \rangle_{L^1, L^\infty(\Omega)} = \langle Z, \mathrm{d}F.\delta \rangle_{\mathbb{R}^{n+1}} = \sum_{i=0}^n z_i \int_{\omega_i} \delta \mathrm{e}^\sigma |\nabla u|^2 + 2\mathrm{e}^\sigma \nabla u \cdot \nabla v \, dx.$$

Using the definition of z this can be written

$$\left\langle \mathrm{d}F^T.Z, \delta \right\rangle_{L^1, L^\infty_0(\Omega)} = \int_\Omega z \delta \mathrm{e}^\sigma |\nabla u(\sigma)|^2 + 2z\mathrm{e}^\sigma \nabla u(\sigma) \cdot \nabla v \, dx.$$

Let us evaluate the second term in the right-hand side. Choosing v as a test function in the adjoint equation satisfied by p, and choosing p as a test function in the equation satisfied by v, we have

$$\int_\Omega z \mathrm{e}^\sigma \nabla u(\sigma) \cdot \nabla v \, dx = \int_\Omega \mathrm{e}^\sigma \nabla p \cdot \nabla v \, dx = \int_\Omega \delta \mathrm{e}^\sigma \nabla p \cdot \nabla u \, dx.$$

Hence for every $\delta \in L^\infty_0(\Omega)$,

$$\langle \mathrm{d}F^T.Z, \delta \rangle_{L^1, L^\infty(\Omega)} = \int_\Omega \left(z \mathrm{e}^\sigma |\nabla u|^2 + 2\mathrm{e}^\sigma \nabla u \cdot \nabla p\right) \delta \, dx.$$

□

3.3. **Local minimisers and degenerate convexity.** We make the following simple observation.

Proposition 3.4. *Assume that σ is such that $E(\sigma) = E(\sigma^\star)$. Then*

$$\left|D^2\mathcal{J}(\sigma)\cdot[\delta,\delta]\right| \leq 2\left\|\frac{d^2j}{ds^2}(E(\sigma^\star),x)\,E(\sigma^\star)\right\|_\infty D^2\mathcal{J}_1(\sigma)\cdot[\delta,\delta], \tag{33}$$

and whenever $\left|\frac{d^2j}{ds^2}(E(\sigma^\star),x)\right|^{-1}$ is integrable we have

$$\left(\int_\Omega\left|\frac{d^2j}{ds^2}(E(\sigma^\star),x)\right|^{-1}dx\right)^{-1}\left(\int_\Omega E\delta dx\right)^2 \leq D^2\mathcal{J}\cdot[\delta,\delta]. \tag{34}$$

When $\mathcal{J}=\mathcal{J}_1$, we have

$$\frac{1}{2}\left(\int_\Omega E(\sigma^\star)\,dx\right)^{-1}\left(\int_\Omega E(\sigma^\star)\,\delta dx\right)^2 \leq D^2\mathcal{J}_1(\sigma)\cdot[\delta,\delta] \leq \frac{1}{2}\int_\Omega E(\sigma^\star)\,\delta^2\,dx.$$

Note that Proposition 3.4 illustrates the fact that it is sufficient to study the case $\mathcal{J}=\mathcal{J}_1$ to prove that degeneracy in the convexity is general. In particular, inequality (33) shows that the Hessian of $\mathcal{J}$ cancels simultaneously as that of $\mathcal{J}_1$, if the energy density is smooth.

The lower bound (34) does not prove strict convexity. However, it provides a rule-of-thumb on how to mend steepest descent algorithm resolutions that tend to stall close to the minimiser. Since $E(\sigma^\star)$ is strictly positive, the lower bound will not vanish if $\delta \geq 0$, or $\delta \leq 0$ everywhere. Therefore, if $\delta^\star$ is the increment given by the algorithm, choosing to alternatively apply either $\max(\delta^\star,0)$ or $\min(\delta^\star,0)$ will avoid a degenerate behaviour.

Proof of Proposition 3.4. Performing the same computation as in the proof of Proposition 3.2, we have for $\sigma\in L^\infty_{\mathrm{ad}}(\Omega)$ and $\delta\in L^\infty_0(\Omega)$,

$$D\mathcal{J}(\sigma)\cdot\delta = \int_\Omega \frac{\partial j}{\partial s}(E(\sigma),x)\,E(\sigma)\left[\delta + 2\frac{\nabla v\cdot\nabla u}{|\nabla u|^2}\right]dx.$$

Another differentiation shows that the second derivative is given by

$$\begin{aligned} D^2\mathcal{J}(\sigma)\cdot[\delta,\delta] &= \int_\Omega \frac{\partial^2 j}{\partial s^2}(E(\sigma),x)\left[E(\sigma)\left(\delta + 2\frac{\nabla v\cdot\nabla u}{|\nabla u|^2}\right)\right]^2 dx \\ &+ \int_\Omega \frac{\partial j}{\partial s}(E(\sigma),x)\,E(\sigma)\left[\delta^2 + 4\delta\frac{\nabla v\cdot\nabla u}{|\nabla u|^2} + 2\frac{\nabla w\cdot\nabla u}{|\nabla u|^2}\right]dx, \end{aligned}$$

where $w\in H^1_0(\Omega)$ is the second derivative of $u(\sigma)$ in the direction δ. When $\frac{\partial j}{\partial s}(E(\sigma),x)\equiv 0$, that is at a critical point of $\mathcal{J}$, this simplifies in

$$D^2\mathcal{J}(\sigma)\cdot[\delta,\delta] = \int_\Omega \frac{d^2 j}{ds^2}(E(\sigma),x)\left[E(\sigma)\left(\delta + 2\frac{\nabla v\cdot\nabla u}{|\nabla u|^2}\right)\right]^2 dx. \tag{35}$$

Note that by construction at the global minimiser, that is, when $E(\sigma)=E(\sigma^\star)$ a.e. in ω, identity (35) holds and $\frac{\partial^2 j}{\partial s^2}(E(\sigma),x)\geq 0$. Therefore,

$$\begin{aligned} \left|D^2\mathcal{J}(\sigma)\cdot[\delta,\delta]\right| &\leq \left\|\frac{d^2j}{ds^2}(E(\sigma^\star),x)\,E(\sigma^\star)\right\|_\infty \int_\omega E(\sigma)\left[\delta + 2\frac{\nabla v\cdot\nabla u}{|\nabla u|^2}\right]^2 dx \\ &\leq 2\left\|\frac{\partial^2 j}{\partial s^2}(E(\sigma^\star),x)\,E(\sigma^\star)\right\|_\infty D^2\mathcal{J}_1(\sigma)\cdot[\delta,\delta], \end{aligned}$$

upon applying formula (35) to

$$j(s,x) = \left(s^{1/2} - E(\sigma^\star, x)^{1/2}\right)^2.$$

This proves the first part of the proposition. Let us now turn to $\mathcal{J}_1$. Expanding $D^2\mathcal{J}_1(\sigma)\cdot[\delta,\delta]$, we find

$$\begin{aligned} D^2\mathcal{J}_1(\sigma)\cdot[\delta,\delta] &= \frac{1}{2}\int_\Omega E(\sigma)\delta^2\,dx + 2\int_\Omega E(\sigma)\left[\frac{\nabla v\cdot\nabla u}{|\nabla u|^2}\right]^2 dx \\ &\quad + 2\int_\Omega \delta\nabla u\cdot\nabla v\,dx, \\ &= \frac{1}{2}\int_\Omega E(\sigma)\delta^2\,dx + 2\int_\Omega \frac{\mathrm{e}^\sigma}{|\nabla u|^2}\Big([\nabla v\cdot\nabla u]^2 - |\nabla v|^2\,|\nabla u|^2\Big)dx, \end{aligned}$$

where we have used (23) with $\varphi = v$. Since, by Cauchy-Schwarz inequality, the second term of the right-hand-side is non positive, we have shown that

$$D^2\mathcal{J}_1(\sigma)\cdot\delta\cdot\delta \le \frac{1}{2}\int_\Omega E(\sigma)\delta^2\,dx.$$

On the other hand, if we choose v as a test function in (20) and integrate by parts, we obtain

$$\int_\Omega E(\sigma)\,\frac{\nabla v\cdot\nabla u}{|\nabla u|^2}\,dx = 0.$$

As a consequence,

$$\begin{aligned} \left(\int_\Omega E(\sigma)\,\delta\,dx\right)^2 &= \left(\int_\Omega E(\sigma)\left[\delta + 2\frac{\nabla v\cdot\nabla u}{|\nabla u|^2}\right]dx\right)^2 \\ &\le D^2\mathcal{J}\cdot[\delta,\delta]\left(2\int_\Omega E(\sigma)\,dx\right), \end{aligned}$$

using again Cauchy-Schwarz inequality. □

The next proposition shows that the Hessian $D^2\mathcal{J}$ is not always positive definite. We provide a counter example in the simplest case, that is, for the Laplacian.

Proposition 3.5. *Let $\Omega := (0,\pi)^2$ and assume that $\sigma \equiv 0$, while $g = x_1$, and $\partial j/\partial s\,(E(0),x) \equiv 0$. Then there exist directions δ such that*

$$\|\delta\|_{L^2(\Omega)} = 1 \quad \text{and} \quad D^2\mathcal{J}(0)[\delta,\delta] = 0.$$

Proof. Since $\sigma = 0$, we have $u := u_1 = x_1$. The corrector $v \in H^1_0$ given by (23) satisfies

$$\Delta v = -\nabla_x\delta. \tag{36}$$

Choose

$$\begin{aligned} \delta(x,y) &= \sum_{n=1}^\infty 2d_n\cos(nx)\sin(ny), \\ &= \sum_{n=1}^\infty d_n\sin(n(x+y)) + \sum_{n=1}^\infty d_n\sin(n(y-x)), \end{aligned}$$

with

$$\frac{\pi}{2}\sum_{n=1}^\infty d_n^2 = 1.$$

An explicit computation gives

$$v(x,y) = -\sum_{n=1}^{\infty} \frac{1}{2n} d_n \sin(nx)\sin(ny),$$

and

$$\delta + 2\frac{\nabla u \cdot \nabla v}{|\nabla u|^2} = 0 \text{ in } \Omega.$$

Therefore, since from formula (35) we have

$$D^2\ \mathcal{J}(0)[\delta,\delta] = \frac{1}{2}\int_\Omega \frac{d^2 j}{ds^2}\,(E(0),x)\left[E(0)\left(\delta + 2\frac{\nabla u\cdot\nabla v}{|\nabla u|^2}\right)\right]^2 dx,$$

the proof is complete. □

Remark: In the proof of Proposition 3.5, we selected an *ad-hoc* family of perturbations, to cancel the Hessian. Had we started with a perturbation of the general form

$$\delta = \sum_{n\geq 0}\sum_{p>0} d_{n,p}\cos(nx)\sin(py),$$

we would have obtained

$$\left(\delta + 2\frac{\nabla u\cdot\nabla v}{|\nabla u|^2}\right)^2 = \sum_{p>0} d_{0,p}^2 \sin^2(py) + \sum_{n>0,p>0} d_{n,p}^2 \left(\frac{n^2-p^2}{n^2+p^2}\right)^2 \cos^2(nx)\sin^2(py).$$

Notice that coefficients in the $\nabla u/|\nabla u| = (1,0)$ direction are not weighted by any factor. Therefore the perturbation, which is the increment in a steepest descent algorithm, is the most important in that direction. This, we think, is an explanation for the speed-up observed in computations, when multiple currents are used, simultaneously or alternatively: the optimisation becomes efficient in multiple directions.

4. Minimisation of the cost function $\mathcal{J}_2$

This section is dedicated to the presentation of the minimisation algorithm for $\mathcal{J}_2$. We do not detail the gradient descent — or steepest descent — algorithm used for $\mathcal{J}_1$. It is a steepest descent algorithm with adaptive step that was implemented using `FreeFem++` [4]. Several boundary conditions are used to estimate the conductivity: $g_1,\dots,g_N$. The cost function is the sum of the cost-functions associated to these boundary conditions: $\mathcal{J}_1 = \sum_{1\leq k\leq N}\mathcal{J}_1^k$.

The optimisation procedures used to minimise the cost function $\mathcal{J}_2$ are detailed. Although we always use Gauss-Newton method, a different approach is followed for fine or coarse computations, which yields in turn a multigrid algorithm, presented in Section 4.2.

4.1. Gauss-Newton optimisation.

We make use of several boundary conditions to estimate the conductivity: $g_1,\dots,g_N$. The cost function is the sum of the cost-functions associated to these boundary conditions: $\mathcal{J}_2 = \sum_{1\leq k\leq N}\mathcal{J}_2^k$.

The domain Ω is divided in subdomains $(\omega_i)_{0\leq i\leq n}$. The true value of the conductivity in ω_0 is assumed to be known. We consider $F:\mathbb{R}^n \to (\mathbb{R}^n)^N$, $\sigma \mapsto (F_1(\sigma),\dots,F_N(\sigma))$, where F_k is associated to the boundary condition g_k and is defined as in equation (26). The map F is C^1 and $\mathrm{d}F = (\mathrm{d}F_1,\dots,\mathrm{d}F_N)$.

The Gauss-Newton Method is an iterative descent method designed to minimise a cost function of the form

$$\mathcal{J}_2(\sigma) = \frac{1}{2}||F(\sigma)||^2 = \sum_{k=1}^{N}||F_k(\sigma)||^2.$$

An initial guess σ^0 is provided, and the m-th iteration reads $\sigma^{m+1} := \sigma^m + \delta^m$, where the descent direction δ^m solves

$$\mathrm{d}F^T.\mathrm{d}F.\delta^m = -\mathrm{d}F^T.F. \tag{37}$$

If the number n of unknowns is small (typically n smaller than 20) the Jacobian matrices $\mathrm{d}F_k$ are computed column-wise by solving n conductivity problems using formula (27). The equation (37) is then assembled and solved easily using any linear solver since $\mathrm{d}F^T.\mathrm{d}F = \sum_{k=1}^N \mathrm{d}F_k^T.\mathrm{d}F_k$ and $\mathrm{d}F^T.F = \sum_{k=1}^N \mathrm{d}F_k^T.F_k$.

If the number of unknowns n is large (for a fine spatial resolution there can be one unknown value of the conductivity in each convex on the finite element mesh) the computation of the full matrix $\mathrm{d}F$ is time and memory consuming. We use an iterative method, namely the conjugate gradient, to solve equation (37) without assembling $\mathrm{d}F$. This requires merely the knowledge of the right-hand side $\mathrm{d}F^T.F$ and a procedure that gives the product of the matrix $\mathrm{d}F^T.\mathrm{d}F$ by a given vector. These are provided by the direct and adjoint differentiations described in paragraph 3.2.

More precisely: $F(\sigma^m)$ is computed by solving N conductivity problems; $\mathrm{d}F^T.F$ is computed by adjoint differentiation (N adjoint problems of conductivity to be solved); and if ξ is given, $\mathrm{d}F^T.\mathrm{d}F\xi = \mathrm{d}F^T.(\mathrm{d}F.\xi)$ is computed in two steps, solving d direct then d adjoint conductivity problems.

We implemented the algorithms that are sketched below:

Algorithm 1: multigrid conductivity estimation (full Jacobian)

input: *the values of the boundary currents $g_1, \ldots, g_N$ and the associated measurements $E_1(\sigma^\star), \ldots, E_N(\sigma^\star)$, initial guess σ^0 (such that $\sigma^0 = \sigma^\star$ in $\Omega \setminus \omega$)*

1.- set $m := 0$,
2.- compute the potentials $u_1, \ldots, u_N$ predicted with the log-conductivity σ^m,
3.- compute $F_k = (f_{k,1}, f_{k,2}, \ldots, f_{k,n})$ where $f_{k,i} = \int_{\omega_i} \mathrm{e}^{\sigma^m} |\nabla u_k|^2 - \int_{\omega_i} E_k(\sigma^\star)$, for $k = 1 \ldots, N$,
4.- compute $\mathrm{d}F_k$, $k = 1 \ldots, N$ column-wise using equation (27),
5.- solve for δ the equation $\left(\sum_{1 \le k \le N} \mathrm{d}F_k^T.\mathrm{d}F_k\right) \delta = -\sum_{1 \le k \le N} \mathrm{d}F_k^T.F_k$,
6.- update the log-conductivity: $\sigma^{m+1} := \sigma^m + \delta$,
7.- if the stopping criterion is not met, set $m := m + 1$ and go to step 2.

Algorithm 2: fine conductivity estimation (zero memory)

Same as algorithm 1 above except:

4.- compute $\mathrm{d}F_k^T.F_k$, $k = 1 \ldots, N$, using equation (31)
5.- solve for δ the equation $\left(\sum_{1 \le k \le N} \mathrm{d}F_k^T.\mathrm{d}F_k\right) \delta = -\sum_{1 \le k \le N} \mathrm{d}F_k^T.F_k$, using conjugate gradient,

4.2. **Multigrid identification of the conductivity.** The conductivity distribution is retrieved from $E_1(\sigma^\star), \ldots, E_N(\sigma^\star)$ by the following multigrid algorithm that is a combination of algorithms 1 and 2.

Algorithm 3: combined algorithm

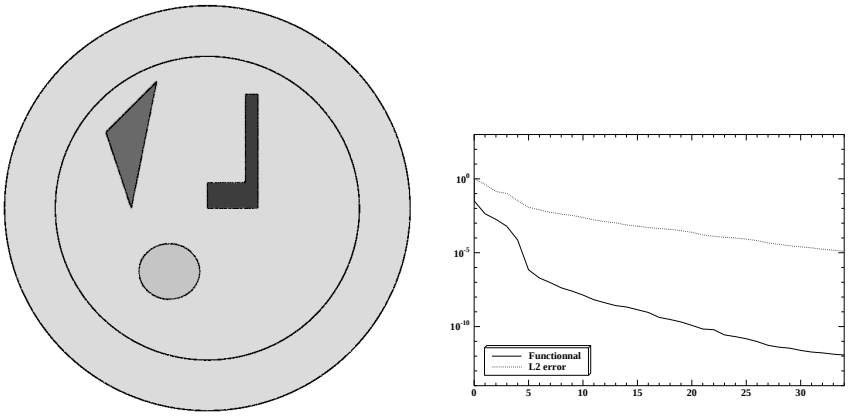

FIGURE 2. The reference material (left) ; the convergence history for the whole domain described in section 5.1 (right)

input: *the discretisation mesh, the values of the boundary currents* $g_1, \dots, g_N$ *and the associated measurements* $E_1(\sigma^\star), \dots, E_N(\sigma^\star)$*, initial guess for the log-conductivity*

1.- set $n := 1$, set $\omega_1 = \omega$, estimate the log-conductivity σ provided by algorithm 1.
2.- define a new partition of Ω by dividing each $(\omega_i)_{1\leq i\leq n}$ in 2 subdomains (that are unions of convexes of the mesh), set $n := 2n$,
3.- find an optimal log-conductivity σ that is constant in each ω_i using algorithm 1.
4.- is n is too large, go to step 5. else go to step 2.
5.- the partition of Ω is the partition defined by the convexes of the mesh,
6.- find the log-conductivity σ that is constant in each convex using algorithm 2.

5. Numerical results using the cost function $\mathcal{J}_1$

In this section, we document the efficiency of the reconstruction method using $\mathcal{J}_1$. Several boundary conditions $g_1, \dots, g_N$ are used to estimate the conductivity. The cost function is the sum of the cost-functions associated to these boundary conditions: $\mathcal{J}_1 = \sum_{1\leq k\leq N} \mathcal{J}_1^k$. A steepest descent algorithm with adaptive step was implemented using `FreeFem++` [4] for the minimisation of $\mathcal{J}_1$. Note that in contrast with the theoretical reconstruction done in Section 2, we only make use of the diagonal data, that is, S_{ii}, $i = 1, \dots, N$, and we make no assumption on the regularity of these data.

We study a test case that was introduced in [2]. On a disk of diameter 1, different conductivities are set, the background conductivity is equal to 0.5, the conductivity in the small disk to 0.75, the one in the triangle to 2 and finally to 2.55 in the L-shaped domain (see Figure 2). On the annulus of inner radius 6 and outer radius 8, the conductivity is supposed known. Dirichlet boundary data are fixed to be equal to the Cartesian coordinates $g_1 = x$, $g_2 = y$, $g_3 = x + y$ and $g_4 = x - y$ on the boundary of the circle.

Note that $S_{33} = S_{11} + S_{22} + 2S_{12}$ and $S_{44} = S_{11} + S_{22} - 2S_{12}$, and the knowledge of this set of four data is actually equivalent to the knowledge of the hypothesis of the theoretical reconstruction done in Section 2.

5.1. **The whole domain.** The first reconstruction test is performed with $\omega = \Omega$, that is, S_{ii}, $i = 1, \dots, 4$ is known everywhere. Figure 2 displays the evolution of the functional $\mathcal{J}_1$ to be minimised and the L^2 error of σ_{comp}, the computed

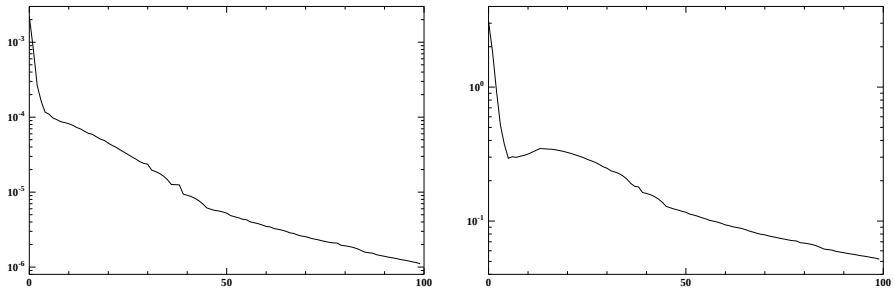

FIGURE 3. The convergence of the cost function $\mathcal{J}_1$ given by (21) (left) and the L^2 error of the conductivity (right).

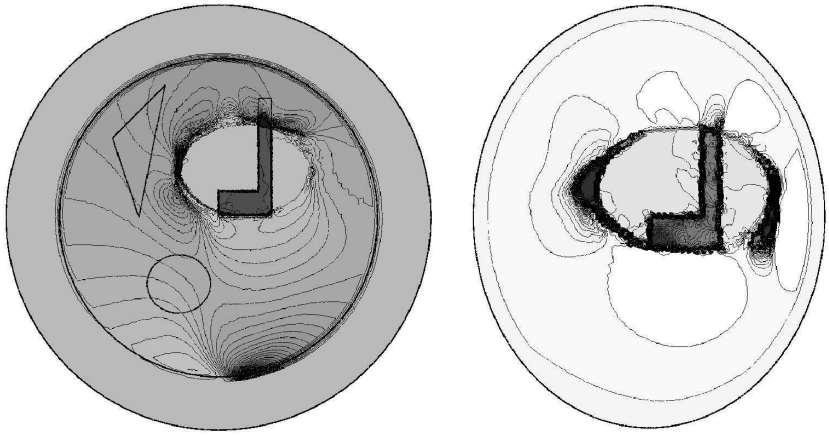

FIGURE 4. The computed conductivity with an ellipse patch, see section 5.2 (left) ; and with an ellipse patch on the wrong domain, see section 5.3 (right).

log-conductivity with $\sigma^\star$ the real log-conductivity. In practical applications, the real conductivity data is unknown: it is presented here to validate the algorithm. Two distinct patterns can be distinguished in the convergence history presented on Figure 2 (right). The first one lies between iterations 1 and 5 and seems quadratic. The second mode happens after iteration 5 and is slower. We believe that this second mode is driven by numerical errors in the resolution of the direct problem and that our algorithm indeed shows quadratic descent. Note that this reconstruction is slower but also converges using one data only, which is impossible using the method presented in [2].

5.2. **Measurements in a smaller domain.** For the second test, the energy density data are available in an ellipse ω around the L-shaped domain. The convergence histories of the cost function and the L^2 difference with the real conductivity are shown in Figure 3. Again, the resulting conductivity approaches well the reference one.

An interesting feature of this test is the tendency of the algorithm to compensate discrepancies of the conductivity outside ω within a boundary layer in the neighbourhood of ω. A close look at Figure 4 (left) shows that the higher conductivity on the left boundary of the ellipse stands for the triangle, and the one on the upper side is the upper branch of the L-shape that is not contained in the ellipse. Note

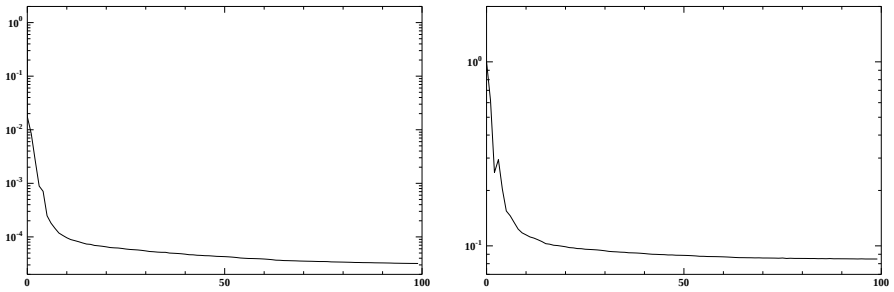

FIGURE 5. The convergence of the functional $\mathcal{J}_1$ (left) and the L^2 difference (right) for the wrong domain of Section 5.3 .

that the computed conductivity is found up to a multiplicative constant: the error graphs were done adjusting this constant.

5.3. **Dependence on the outer-domain for interior patches.** The experiment conducted in Subsection 5.2 and the theoretical reconstruction in Section 2 illustrate that if the value of S_{ii} is known within ω, then the value of σ can be retrieved within ω. A natural question is whether such a reconstruction is still possible when the domain Ω, and the Dirichlet boundary data g_i is only approximately known. Section 2 indicates that this is not a necessary prior and in real experiments the domain Ω will not be very precisely defined – the external shape of soft material may vary. In this test, the elliptic measurement subdomain is preserved, but we attempt to recover σ with a domain Ω that has been changed into a smaller ellipse. The Dirichlet boundary data imposed are the Cartesian coordinates data g_i previously used, x, y, $x+y$, $x-y$, but they are now imposed on this new domain. Because they are not the $\sigma^\star$-harmonic extensions of the previous boundary conditions, an error is introduced in the boundary conditions.

The computed conductivity σ_{comp} is given in Figure 4 (right) and the convergence history in Figure 5. The algorithm compensates for the discrepancies outside ω and finds the conductivity σ_{comp} up to a constant. For the L^2 difference, σ_{comp} has been renormalised with the best constant.

5.4. **Solving with a patchwork approach.** The previous tests show that the conductivity can be recovered within a "patch", a sub-region of the domain. We now investigate whether the algorithm can be parallelised with multiple computers recovering different patches. Since no constraint is imposed on the conductivity outside the area of interest, Figure 3 shows that the minimisation procedure tends to create important errors outside the optimised patch ω, in a boundary layer surrounding ω. A natural concern is whether these error would render parallelisation inefficient.

The following numerical trial is an attempt to address this question. We optimise successively on two overlapping patches. Figure 6 shows the resulting conductivities when the algorithm is applied with the right patch only, then with the left patch only, and then when the algorithm take each patch into account every two iterations.

Figure 7 shows the convergence history. On the right is the evolution of the cost function associated with the two subdomains corresponding to the two patches. It is compared to the convergence history of the cost functions when the full ellipse is taken into account for optimisation. On the left is the evolution of the cost function corresponding to one single patch (the left one), also compared with the alternate optimisation iterations.

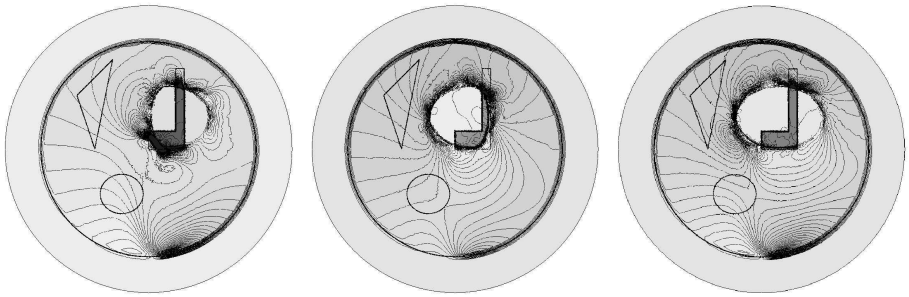

FIGURE 6. The computed conductivity with the right patch only, the left one only, and then successive patches.

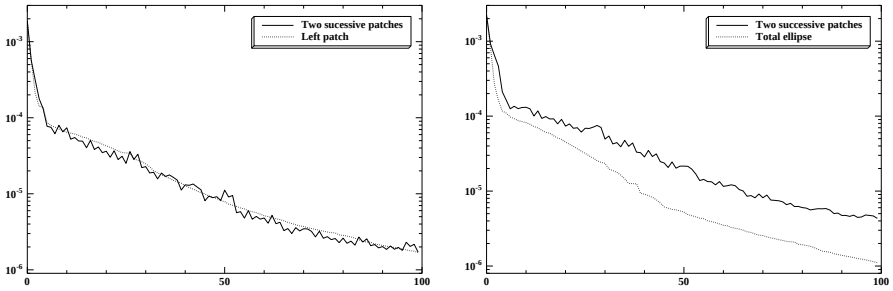

FIGURE 7. The convergence of the cost function $\mathcal{J}_1$ corresponding to the ellipse (right) and the right patch (left) in the successive patches algorithm. They both are compared to the convergence history of the algorithm when the whole ellipse or only the right patch are taken into account

Those convergence histories show that optimising independently each region is not as efficient as a global minimisation algorithm. However, it is not less efficient than the optimisation on any of the two sub-regions. This shows that the error boundary layer which appear on the boundary of the patches is not a severe drift from the optimal solution, as it vanishes when the outside domain is updated. The parallelisation of the algorithm is therefore relatively simple. For each given patch, the outside medium simply needs to be updated regularly by the results obtained on other patches.

6. Numerical results using the cost function $\mathcal{J}_2$

In this section, the numerical results obtained for the cost function $\mathcal{J}_2$ are presented. Several boundary conditions $g_1, \ldots, g_N$ are used to estimate the conductivity. The cost function is the sum of the cost-functions associated to these boundary conditions: $\mathcal{J}_2 = \sum_{1 \leq k \leq N} \mathcal{J}_2^k$. The algorithms were implemented with piecewise linear finite elements, using `Getfem++` [6] and Matlab. The results presented below were obtained with the multigrid algorithm introduced in Section 4.2.

6.1. **Two dimensional results: a half-disk.** The domain $\Omega \subset \mathbb{R}^2$ is a half disk of radius 1 centered at the origin, the conductivity σ is unknown in the half disk ω of radius 0.9 centered at the origin. The domain Ω is meshed by 5168 triangles and 2647 vertices. The subdomain ω contains 4253 convexes, this is the number of unknowns, and the number of data for each boundary current applied.

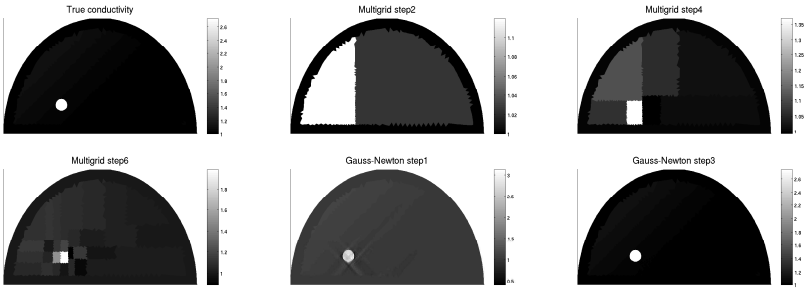

FIGURE 8. From left to right, first row: True conductivity ; multigrid step 2 ; multigrid step 4. Second row: multigrid step 6 (left). The last two computations are on the fine grid: Gauss-Newton step 1 (centre) and Gauss-Newton step 3 (right).

There are $N = 2$ different boundary currents, respectively equal to x_1 and x_2 (the spatial coordinates) but for the bottom boundary of the domain that is considered as insulating (homogeneous Neumann condition). In figure 8 the true conductivity (top left) and the estimated conductivity at several steps of algorithm are presented.

6.2. **Three dimensional results: a half-sphere.** A more realistic three dimensional geometry was simulated, in order to mimic breast examination. The domain Ω is a half-sphere of radius 1.1, the domain ω is a half sphere of radius 0.9. The mesh of the domain ω contains 4710 convexes, this is the number of unknown conductivity coefficients.

The bottom of the half sphere is insulating (homogeneous Neumann condition), and there are 8 disk-shaped electrodes at the boundary, see figure 9. One experiment consists of applying a Dirichlet condition to the electrodes, such that each electrode is at a given electric potential. The true conductivity $e^{\sigma^\star}$ is space-dependent, there is a spherical inclusion of radius 0.1 with high conductivity and a background where the conductivity depends smoothly on the second space variable. The quantity $e^{\sigma^\star}|\nabla u^\star|^2$ is measured in ω.

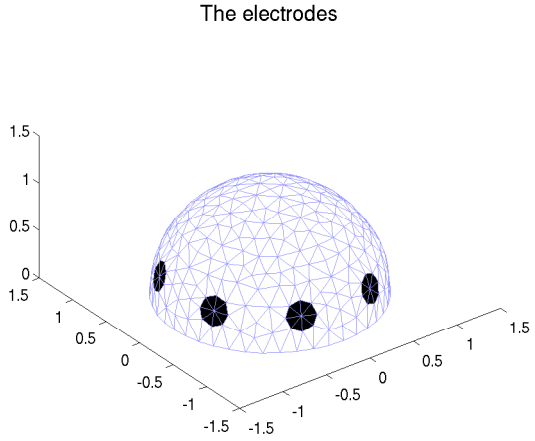

FIGURE 9. Location of the electrodes (black circles)

There are $N = 4$ boundary conditions defined as follows: on each electrode a potential equal to respectively $g_1 = x_1$, $g_2 = x_2$, $g_3 = x_1 + x_2$ and $g_4 = x_1 - x_2$.

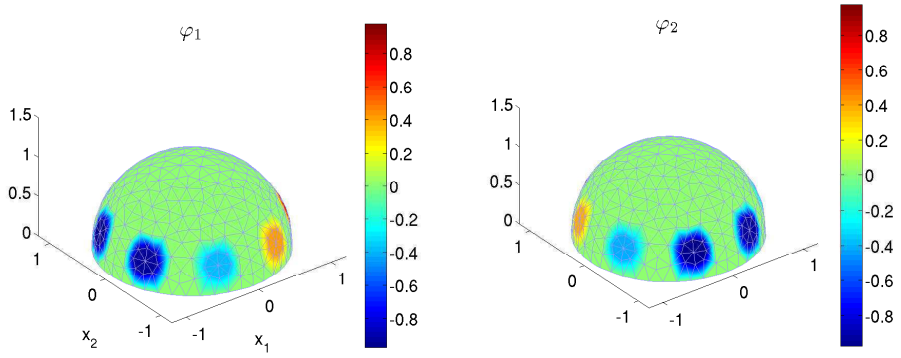

FIGURE 10. The boundary conditions g_1 (left) and g_2 (right)

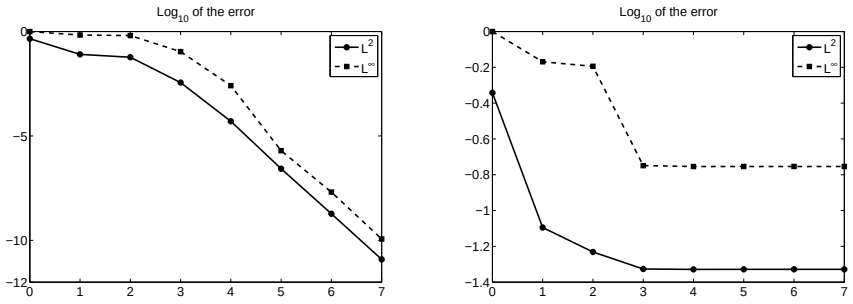

FIGURE 11. Evolution of the $\log_{10}$ of the discrepancy between the true and the reconstructed conductivity: no noise (left) and 2% noise (right)

where x_1 and x_2 are the first and second spatial coordinate of the centre of mass of the electrode. We show g_1 and g_2 on figure 10.

The multigrid algorithm described in paragraph 4.2 was applied with the following parameters: two coarse multigrid steps and five fine Gauss-Newton steps. Figure 11 shows the logarithmic evolution of the discrepancy between the true conductivity and the reconstructed conductivity, as a function of the iterations (measured with different norms), with no noise and with 2% noise. The complete resolution takes about 600s with a 1.73 GHz computer.

Note: other simulations were conducted with less boundary conditions ($N = 2$). In the absence of noise, the results of the reconstruction were analogous to the reconstruction with $N = 4$ different boundary conditions (but the speed is twice faster since the total number of conductivity problems to be solved is divided by a factor 2). However, in the presence of noise, taking into consideration 4 measurements allows to reduce the variance of the noise (and hence the error in the retrieved conductivity). An application to real data should evaluate the number of experiments that provides the best trade-off between speed and noise variance reduction.

Acknowledgement. This paper is the result of a collaboration which happened when all the authors were in Versailles. This was made possible by the ANR project EchoScan (AN-06-Blan-0089). All the authors benefited from this grant, and gratefully acknowledge the support it provided.

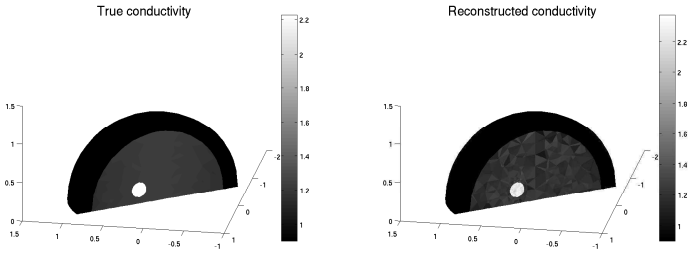

FIGURE 12. Slice views of the true and the reconstructed conductivity with 2% noise

REFERENCES

[1] G. Alessandrini and V. Nesi. Univalent σ-harmonic mappings. *Arch. Rat. Mech. Anal.*, 158:155–171, 2001.

[2] H. Ammari, E. Bonnetier, Y. Capdeboscq, M. Tanter, and M. Fink. Electrical impedance tomography by elastic deformation. *Submitted*, 2007.

[3] M. Briane, G. W. Milton, and V. Nesi. Change of sign of the corrector's determinant for homogenization in three-dimensional conductivity. *Arch. Ration. Mech. Anal.*, 173(1):133–150, 2004.

[4] F. Hecht, O. Pironneau, A. Le Hyaric, and K. Ohtsuka. *FreeFem++*. Laboratoire Jacques-Louis Lions, UMR 7598, 2.20 edition, 2007.

[5] R. S. Laugesen. Injectivity can fail for higher-dimensional harmonic extensions. *Complex Variables Theory Appl.*, 28(4):357–369, 1996.

[6] Y. Renard and J. Pommier. *Getfem++, a generic Finite Element library in C++*. Laboratoire MIP, UMR 5640, 2007.

MATHEMATICAL INSTITUTE, UNIVERSITY OF OXFORD, OXFORD OX1 3LB, UK
E-mail address: YVES.CAPDEBOSCQ@MATHS.OX.AC.UK

LMV, UNIVERSITÉ VERSAILLES-SAINT QUENTIN, CNRS, VERSAILLES, FRANCE
E-mail address: FREDERIC.DE.GOURNAY@UVSQ.FR

IMT, UNIVERSITÉ PAUL SABATIER, CNRS, TOULOUSE, FRANCE
E-mail address: FEHREN@MIP.UPS-TLSE.FR

LMV, UNIVERSITÉ VERSAILLES-SAINT QUENTIN, CNRS, VERSAILLES, FRANCE
E-mail address: OTARED.KAVIAN@UVSQ.FR